Photofragment translational spectroscopy of propargyl radicals at 248 nm

Scott J. Goncher, David T. Moore,[†] Niels E. Sveum,[‡] Daniel M. Neumark[*]

Department of Chemistry, University of California, Berkeley, CA 94720, USA, and Chemical Sciences Division, Lawrence Berkeley National Laboratory, Berkeley, CA 94720, USA.

Abstract

The photodissociation of propargyl radical, C_3H_3, and its perdeuterated isotopolog was investigated using photofragment translational spectroscopy. Propargyl radicals were produced by 193 nm photolysis of allene entrained in a molecular beam expansion, and then photodissociated at 248 nm. Photofragment time-of-flight spectra were measured at a series of laboratory angles using electron impact ionization coupled to a mass spectrometer. Data for ion masses corresponding to $C_3H_2^+$, C_3H^+, C_3^+, and the analogous deuterated species show that both H and H_2 loss occur. The translational energy distributions for these processes have average values $\langle E_T \rangle$ = 5.7 and 15.9 kcal/mol, respectively, and are consistent with dissociation on the ground state following internal conversion, with no exit barrier for H loss but a tight transition state for H_2 loss. Our translational energy distribution for H atom loss is similar to that in previous work on propargyl in which the H atom, rather than the heavy fragment, was detected. The branching ratio for H loss/H_2 loss was determined to be 97.6/2.4 ± 1.2, in good agreement with RRKM results.

[†] Current address: Department of Chemistry, Lehigh University, Bethlehem, PA 18015
[‡] Intel Corporation, 2501 NW 229th Avenue, Hillsboro, OR 97124
[*] Corresponding author. Email: dneumark@berkeley.edu

I. Introduction

The propargyl radical is the most stable isomer on the C_3H_3 potential energy surface and plays important roles in reactions involving small hydrocarbon intermediates, including combustion and interstellar chemistry.[1-3] The bimolecular reaction of two propargyl radicals produces an aromatic ring which may serve as key precursor to formation of polyaromatic hydrocarbons and soot.[4-6] The radical itself has been studied extensively by an array of experimental methods. Its ground electronic state has been characterized by microwave[7] and infrared spectroscopy,[8,9] and two electronic bands[10-12] in the ultraviolet (UV) have been assigned to propargyl. Its electron affinity has been determined by anion photoelectron spectroscopy,[13,14] and its ionization potential has been measured by electron impact,[15] photoelectron spectroscopy,[16] and zero electron kinetic energy spectroscopy.[17] Several laboratories have investigated the photodissociation dynamics of propargyl in order to investigate its primary photochemistry.[18-20] Theoretical studies of propargyl have focused on its structure and energetics, the topology of its ground state potential energy surface with respect to both isomerization and dissociation, and its low-lying excited states.[21-29] Some of this work[27,28] has questioned the assignment of the UV absorption band around 242 nm to propargyl and thus, the validity of the photodissociation experiment done at this wavelength, motivating the experiments reported here in which we perform photofragment translational spectroscopy on propargyl at 248 nm.

Excitation of propargyl in the ultraviolet can access several dissociation channels involving multiple isomers. There are three close-lying H atom loss channels (energies in kcal/mol):

$$HCCCH_2 + h\nu \rightarrow c\text{-}C_3H_2 + H \qquad \Delta H_0 = 85.6 \qquad (1a)$$

$\rightarrow$ HCCCH (^{3}B) + H $\quad \Delta H_0 = 100.1$ (1b)

$\rightarrow$ $CCCH_2$ + H $\quad \Delta H_0 = 100.6$ (1c).

There also exists an H_2 loss channel,

$HCCCH_2 + h\nu \rightarrow C_3H + H_2 \quad \Delta H_0 = 88.5$ (2)

The changes in enthalpy for the above reactions were calculated using the heats of formation determined by Nguyen *et al*[25] that represent a combination of both experiment and theory.[30] The energetics for reaction 2 assume the C_3H fragment is formed in its quasi-linear isomer; there is also a nearly isoenergetic cyclic isomer.[31,32]

Fahr et al[11,12] have identified a relatively strong absorption from 230-250 nm with a maximum around 240 nm from fragments produced by photolysis of either propargyl chloride or allene at 193 nm. This absorption was assigned to the $\tilde{B}\ ^2B_1 \leftarrow \tilde{X}\ ^2B_1$ transition of propargyl based on electronic structure calculations at various levels of theory. This observation facilitated an experimental investigation by Deyerl *et al*[19] of propargyl photodissociation at 242 nm. In these studies, supersonic flash pyrolysis of propargyl bromide was used to produce internally cold propargyl radicals. The radicals were photodissociated and the H atom products were ionized by Lyman-α radiation at 121 nm. One-dimensional Doppler profiles for H-atom ionization were analyzed to recover the photofragment translational energy probability distribution, $P(E_T)$. The form of this distribution suggests a mechanism in which electronic excitation is followed by internal conversion to the ground state and statistical decay to products. Based on the observed energetics and previous studies of similar small hydrocarbons, the authors concluded that the most likely H loss product was cyclopropenylidene (reaction 1a). This conclusion was supported by photodissociation studies of isotopically substituted propargyl ($D_2C{=}C{=}C{-}H$)

radicals that showed complete scrambling of the H and D photoproducts, suggesting that the reaction proceeded through a cyclic intermediate.

Further insight into the unimolecular dissociation of propargyl derives from theoretical work by Nguyen et al.[25,26] An extensive, high-level computational study of the C_3H_3 surface,[25] followed by RRKM rate-constant calculations,[26] identified several dissociation channels and the branching ratios associated with those channels. The H atom loss channels (reaction 1) all have dissociation pathways without reverse activation (exit) barriers, while H_2 loss (reaction 2) proceeds through a transition state to dissociation lying 10.2 kcal/mol above the products. Although formation of the cyclopropenylidene (reaction 1a) fragment is the most energetically favorable of the H loss channels, the RRKM analysis predicted that 90.2% of 242 nm photodissociation results in propargylene production (reaction 1b), in apparent disagreement with Deyerl *et al*, and that isotopic scrambling, which was used as evidence for production of the cyclic isomer, occurs through various isomerization pathways prior to H atom loss. The H_2 loss channel, which could not be seen by Deyerl *et al*, is predicted to contribute only 3.0% to photodissociation products. Similar H/H_2 branching ratios were calculated at 193 nm, in apparent agreement with results by Jackson *et al*[18] in a study on allene photodissociation in which the propargyl radical product was dissociated by absorption of a second photon.

Recent high-level theoretical calculations by Eisfeld[27,28] find that although propargyl radical does have an absorption near 240 nm, it is vibronically allowed but dipole-forbidden, and therefore too weak to explain the experimental results. Based on these calculations, Eisfeld proposed that neither the absorption band from 230-250 nm nor

the photodissociation experiment by Deyerl *et al* probed the propargyl radical and that, for example, the H atom fragments measured by Deyerl *et al* came from a different species.

A recent study by McCunn *et al*[20] investigated secondary dissociation of propargyl produced by the 157 nm photodissociation of propargyl chloride. The authors observed secondary photofragments consistent with the loss of both H-atoms and molecular H_2 from propargyl radical. Based on the differences between chlorine fragment and propargyl fragment $P(E_T)$ distributions, they claimed that propargyl radicals with internal energies greater than 71.5 +5/-10 kcal/mol will undergo unimolecular dissociation. This value is more than 10 kcal/mol lower than any of the calculated dissociation channels for propargyl radical.[18,33,34]

The current study employs photofragment translational spectroscopy[20] to investigate the 248 nm photodissociation of propargyl radicals produced in a molecular beam photolysis source in which allene is photodissociated at 193 nm. Previous studies showed that propargyl is indeed the primary 193 nm photoproduct of allene, with a yield of ~95% in a collision-free environment.[18,35] Furthermore, allene has a very small absorption cross section at 248 nm,[36] so any 248 nm photodissociation signal should be specific to propargyl radical. This study is complementary to the previous work by Deyerl,[19] since we detect the heavy fragments (C_3H_2, etc) produced at 248 nm. A comparison of the resulting heavy fragment $P(E_T)$ distribution with that obtained by their Doppler analysis of the H atom loss channel would confirm that both experiments are measuring signal from propargyl photodissociation. We find that this is indeed the case. Our results also show evidence for a minor H_2 loss channel. The consistency of our results and analysis is confirmed through photodissociation measurements on C_3D_3 at 248 nm.

II. Experimental

The main features of the photofragment translational spectroscopy apparatus has been described in detail previously.[37,38] Figure 1 shows the modifications needed to study the photodissociation of reactive free radicals. Briefly, radicals were generated by allene photolysis at 193 nm and photodissociated at 248 nm. Photofragments were then detected at various laboratory scattering angles, Θ_{lab}, by a rotating mass spectrometer.

Propargyl radicals were generated by 193 nm supersonic flash-photolysis of allene. Normal or perdeuterated allene (C/D/N Isotopes, 98 %) was seeded in He carrier gas at 5% concentration, and expanded through a piezoelectrically actuated pulsed valve with a backing pressure of ~700 Torr. The molecular beam intersected an 18 ns pulse of 193 nm light (GAM, EX100) focused to a 3 x 1 mm spot about 1 mm downstream from the valve orifice, with the goal of maximizing collisional cooling and entrainment in the beam of the radicals produced by the photolysis pulse. The molecular beam then passed through two collimating skimmers into a differentially pumped region, where it was crossed by a 248 nm excimer laser pulse (Lambda Physik LPX 220i) focused to a 2 x 4 mm spot; this interaction region lay 9.8 cm downstream from the point of intersection with the 193 nm pulse. The pulsed valve and 248 nm excimer laser were triggered at 200 Hz, while the 193 nm laser was triggered at 100 Hz. This procedure allowed for subtraction of background that arises from dissociative ionization in the mass spectrometer of allene parent, which was particularly pronounced at small Θ_{lab}, as well as any allene photodissociation from the 248 nm pulse.

Photofragments scattered in the plane of the molecular and laser beams were detected as a function of Θ_{lab} using a rotatable, triply differentially pumped mass

spectrometer.[39] After passing through three collimating apertures, the photofragments were ionized by electron impact (80 eV), mass selected with a quadrupole mass filter, and detected with a Daly-style detector. Ionized photoproducts were counted as a function of time from the 248 nm photodissociation pulse by means of a multichannel scaler interfaced to a computer, yielding a photofragment time-of-flight (TOF) distribution for a specific mass-to-charge ratio (*m/e*). The flight distance between the 248 nm laser interaction region and the ionizer was 20.8 cm and all measured TOF distributions were adjusted for the ion flight time through the ionizer. In these experiments, ion signal at *m/e* =38 ($C_3H_2^+$), 37 (C_3H^+) and 36 (C_3^+) was measured for C_3H_3 experiments, and at *m/e* = 40 ($C_3D_2^+$), 38 (C_3D^+) and 36 (C_3^+) for the C_3D_3 experiments. TOF distributions were analyzed using forward-convolution programs designed to simulate TOF spectra based on the center-of-mass translational energy distribution of the photofragments.

The speed distribution of the allene parent molecule was characterized using a retractable chopper wheel, located after the second collimating skimmer, to modulate the molecular beam. This chopper wheel was used in the full photodissociation experiment as well, serving as the "master clock" for timing the 193 and 248 nm laser pulses. Timing of the 193 nm laser pulse was adjusted manually to optimize the overlap of the irradiated portion of the molecular beam with the chopper slit. The number of photodissociated allene molecules was monitored by measuring the difference in the molecular beams with the 193 nm laser on and off. Spatial and temporal alignment was achieved by maximizing this difference. The photolysis of the parent molecule resulted in a "depletion hole" in the subtracted signal, which scaled roughly linearly with the fluence of the 193 nm light; 10-18% depletion using ~6 mJ/mm^2 was typical for optimal timing. Timing of the 248 nm

pulse required characterization of the propargyl radical speed distribution using the following procedure.

In a typical photodissociation experiment of a stable molecule, measurement of the parent molecule speed distribution is performed by setting the detector to $\Theta_{lab} = 0^{o}$, and measuring the TOF distribution of the parent beam from the chopper to the detector. The distribution is then fit to the functional form oft used for speed distributions of supersonic beams:[37,40,41]

$$N(v) = v^2 \exp\left[-s^2\left(\frac{v}{V_0} - 1\right)^2\right] \qquad (3)$$

Here, V_0,the flow velocity, is used to determine the timing of the photodissociation laser, while s, the speed ratio, is given by $V_0 / \Delta v$, where Δv is the beam velocity spread. Typically, an allene beam seeded in He would have beam parameters $V_0 \approx 1500$ $^{m}/_{s}$, and $s \approx 13$. While one might expect similar parameters for propargyl radical entrained in the same beam, the extent of entrainment and translational cooling of the propargyl is unknown, so an independent measurement of V_0 and s is desirable. One cannot simply measure the propargyl speed distribution at $\Theta_{lab} = 0^{o}$ because the $C_3H_3^+$ parent ion signal is swamped by dissociative ionization of the allene beam.

Instead, once the 193 nm laser timing was established, the detector was rotated to $\Theta_{lab} = 10^{o}$, and the propargyl radical photodissociation signal at one of the photofragment masses was monitored as a function of Δt, the delay between the 193 and 248 nm laser pulses. The average velocity of the radicals sampled by the 248 nm pulse is given by 9.8 cm/Δt, where 9.8 cm is the distance between the laser spots. An initial value of Δt was

calculated from the parent beam velocity. This timing was then varied over the entire width of the propargyl pulse coming through the chopper hole, and the total photodissociation signal at each Δt was determined by integrating the photofragment TOF distribution. Figure 2 shows the resulting velocity distribution measured for the propargyl radicals. Each data point in this figure represents the total $m/e = 37$ dissociation signal of 20,000 laser shots. The propargyl speed distribution obtained in this way is quite similar to that for the parent beam and is fit to the same functional form that would be used for a stable molecule (equation 3), convoluted over appropriate instrument parameters. For the data in Fig. 3, $V_0 = 1535$ m/s and $s = 11$, which are quite comparable to the values for the allene parent beam.

III. Results

Figure 3 shows representative TOF spectra at several laboratory angles for ion signal at $m/e = 38$, $C_3H_2^+$, while Fig. 4 shows TOF spectra at $m/e = 37$ (C_3H^+) and $m/e = 36$ (C_3^+). The $C_3H_2^+$ signal comes only from ionization of the C_3H_2 fragment from the H loss channel, reaction 1, whereas the $m/e = 37$ TOF spectra include contributions from both C_3H fragments from H_2 loss (reaction 2) and dissociative ionization of C_3H_2 fragments. Signal at $m/e = 36$ can arise from dissociative ionization of C_3H_2 and C_3H; neutral C_3, the other possible contributor to this ion mass, is not accessible by one-photon dissociation of C_3H_3, and no evidence for C_3 production (by two-photon absorption, for example) is seen. In all TOF spectra, the open circles represent the data and the various lines represent forward convolution simulations of the experiment based on center-of-mass translational energy $P(E_T)$ distributions (see Section IV).

Even in the presence of extensive dissociative ionization, measurement of TOF spectra at various ion masses as a function of Θ_{lab} enables one to distinguish the contributions from reactions 1 and 2 to the signal at *m/e* = 37 and 36. Figure 5 shows a representative Newton diagram for the C_3H_2 and C_3H fragments. In this diagram, the laboratory frame velocity of the propargyl radical (represented by the solid black arrow) is set to be 1535 m/s based on Fig. 2. Each circle represents the locus of center-of-mass velocity vectors for the detected fragment assuming no product internal excitation (i.e. maximum translational energy). This diagram was constructed using the energetics determined by Nguyen *et al.*[25] The solid black circle and grey circles correspond to the C_3H_2 fragments from reactions 1a and 1b, respectively, and the dotted black circle corresponds to C_3H fragments produced in reaction 2. The Newton diagram shows the maximum Θ_{lab} at which a particular channel can be observed and, as expected, this angle is considerably larger for reaction 2 than for the H atom loss channels.

We find that no signal at *m/e* = 38 is detected at $\Theta_{lab} > 15^{o}$, while Fig. 3 shows that TOF spectra at *m/e* = 37 and 36 spectra can be measured at larger angles (such as Θ_{lab} = 20^{o}, as shown in Fig. 3). The signal at these larger angles must come from C_3H produced by reaction 2 rather than dissociative ionization of C_3H_2. Therefore, at least two dissociation processes are occurring: H loss, evidenced by the peak in the *m/e* = 38 TOF spectra and at small scattering angles in the *m/e* = 36 and 37 spectra, and H_2 loss, demonstrated by the signal found only in the *m/e* = 37 and 36 TOF spectra. Figure 4 shows that at 20°, where only products from reaction 2 are seen, the TOF spectra is more than an order of magnitude less intense than the data at the two smaller angles, suggesting that

reaction 2 is a minor channel; this is borne out by the more quantitative analysis outlined in Section IV.

Experiments were also performed on perdeuterated propargyl ($D_2C=C=CD$), generated from the 193 nm photolysis of perdeuterated allene. Data were taken at *m/e* = 40 ($C_3D_2^+$), 38 (C_3D^+), and 36 (C_3^+) fragments in 2.5° intervals of Θ_{lab} = 7.5° – 20°. Figure 6 shows representative TOF spectra for *m/e* = 38 (C_3D^+) over a range of laboratory angles. All deuterated fragment TOF spectra show a single featureless peak resembling the TOF spectra of the nondeuterated species. However, C_3D_2 signal is seen over a wider angular range. This result is expected, as the kinematics in the deuterated system require all heavy photofragments to have greater center-of-mass velocity than their nondeuterated counterpart.

No scattering signal was observed with the mass filter set for detection of any higher *m/e*, including *m/e* = 39 ($C_3H_3^+$). It has been shown that hot allene molecules will absorb light at 248 nm.[42] Because allene is being used a precursor, it was possible that photodissociation signal could arise from the absorption of allene that vibrationally excited from the 193 nm laser. However, the fact that no *m/e* = 39 signal was observed indicates that there is little or no contamination in the data from 248 nm photodissociation of hot allene molecules. These observations also indicate that the observed signal is not from photodissociation of possible propargyl radical self-reaction products in the beam, since this process would presumably result in some fragments with greater mass than C_3H_2.

IV. Analysis

The joint photofragment energy and angular distribution, $P(E_T,\theta)$, is given for each dissociation channel by

$$P(E_T,\theta) = P(E_T)I(\theta)$$

where $P(E_T)$ and $I(\theta)$ are the uncoupled center-of-mass translational energy and angular distributions, respectively. The $P(E_T,\theta)$ distribution for each reaction channel was determined by fitting all the measured TOF spectra of the dissociation fragments. The TOF spectra were fit using the PHOTRAN[43] forward convolution program. A simulation of all the measured TOF spectra was generated using an input $P(E_T)$ distribution which is then convoluted over various instrument parameters. Beam velocity, laboratory angle, dissociation and ionization volumes, finite angular acceptance angle of the detector, laser power, and polarization angle were all accounted for in the convolution. The $P(E_T)$ distribution was adjusted until the best simultaneous fit of all TOF data was achieved. Although the excimer laser used in these experiments was not polarized, the configuration of the experimental apparatus, in which the direction of laser propagation is in the plane defined by the molecular beam and the detector, allows for an anisotropic photofragment angular distribution in the plane of detection. However, a satisfactory fit to the data was obtained assuming an isotropic distribution.

The best fit to the TOF data was achieved using the $P(E_T)$ distributions in Figs. 7a and 8 for H and H_2 loss, respectively, with relative weighting of the two distributions discussed further below; the $P(E_T)$ distribution in Fig. 7b, taken from Deyerl *et al*,[19] is considered in Section V. Contributions to the TOF spectra from the $P(E_T)$ distribution in Fig. 7a are shown as grey lines in Figs. 3, 4 and 6, whereas those from Fig. 8 are shown

as dashed lines in Figs. 4 and 6. Black lines in Figs. 3, 4, and 6 indicate the sum of the two contributions and are not shown when only a single component is needed to simulate a range of data points. In Fig. 4, we see that H loss is the dominant contribution to the TOF spectra at 10° and 12.5°, but that the TOF spectra at 20° result entirely from H_2 loss. An excellent fit to the data in Fig. 6 from C_3D_3 dissociation is obtained using the same $P(E_T)$ distributions, even though the kinematics of reactions 1 and 2 for C_3D_3 are quite different, thus supporting the validity of our analysis.

The $P(E_T)$ distribution of the C_3H_2 fragments is peaked near zero ($E_{T,peak}$ = 1.8 kcal/mol), with an average translational energy $\langle E_T \rangle$ = 5.7 kcal/mol, and spans the entire range of available energy for C_3H_2 + H products (0 – 29.7 kcal/mol). Figure 7 also shows the maximum translational energy release possible for both the HCCCH + H and c-C_3H_2 + H fragmentation pathways for dissociation at 248 nm. Most fragments are produced with translational energies below the maximum allowed for the HCCCH + H channel, $E_T \leq$ 15.2 kcal/mol; a small fraction extends beyond this limit but not beyond the translational energy maximum of 29.7 kcal/mol for c-C_3H_2 + H.

The $P(E_T)$ distribution for C_3H + H_2 in Fig. 8 is peaked both well away from zero, ($E_{T,peak}$ = 14.6 kcal/mol) and close to the translational energy expectation value, ($\langle E_T \rangle$ = 15.3 kcal/mol). These features are distinct from the H loss $P(E_T)$ distribution shown in Fig. 7 indicating a different dissociation mechanism is occurring. The error bars for this distribution are large for $E_T \leq$ 11 kcal/mol, because fragments in this kinetic energy range are seen only at small Θ_{lab} where dissociative ionization of C_3H_2 dominates.

From our data, the intrachannel branching ratio can be obtained from the data for H loss versus H_2 loss. This branching ratio can be obtained from the signal levels in the

laboratory TOF spectra, following normalization by electron impact cross section of the fragments and the number of laser shots. Electron impact cross sections were estimated using atomic ionization cross section additivity scheme of Fitch and Sauter.[44,45] The fitting program used to simulate the TOF spectra returns the relative weights of the $P(E_T)$ distributions needed to reproduce the relative signal intensities of the TOF spectra for each channel. The intrachannel branching ratio for H loss/H_2 loss is 97.6/2.4 ± 1.2, a result in good agreement with previous RRKM analysis.[26]

V. Discussion

One motivation of our experiments was to investigate whether Deyerl *et al*[19] were in fact probing H atom loss from the propargyl radical or, if instead, as suggested by Eisfeld,[27,28] the H atoms detected in their experiment came from the photodissociation of a different species. Our results for reaction 1 are complementary to the H atom study because we detect the C_3H_2 counterfragment. At the same excitation energy, the derived $P(E_T)$ distributions should be identical for both H and C_3H_2 photofragments because the two are momentum-matched.

Fig. 7 shows a side-by-side comparison of the $P(E_T)$ distributions from the two experiments. Since the experiments were done at slightly different wavelengths (248 vs. 242 nm), it is also useful to compare the corresponding $P(E_{int})$ distributions, where E_{int}, the internal energy of the C_3H_2 fragment, is given by

$$E_{\text{int}} = h\nu - E_T - D_0 . \qquad (4)$$

D_0 is the dissociation energy to the lowest energy products, c-C_3H_2 + H. The $P(E_{int})$ distributions are obtained by referring the curves in Figs. 7a and 7b to the top axes in both

panels. The two distributions are very similar. Both peak near $E_T = 0$, and the average fragment internal energy in our distribution, $\langle E_{int} \rangle = 109.9$ kcal/mol, is only slightly greater than the value of 109.1 kcal/mol obtained by Deyerl *et al.* This small discrepancy may reflect the slightly lower photon energy in our experiment or differences in the internal temperatures of the radicals produced in the two experiments. Nonetheless, the strong similarity between our two complementary measurements supports the previous attribution of this signal to propargyl photodissociation. The form of the $P(E_T)$ distributions in Fig. 7, peaking near $E_T = 0$, is what would be expected for a overall mechanism in which internal conversion occurs to the ground electronic state, followed by dissociation through a loose transition state with no exit barrier.

There does, however, remain some ambiguity as to the identity of the C_3H_2 fragments. Deyerl *et al* attributed the measured fragments to c-C_3H_2 + H (reaction 1a), while RRKM analysis[26] found HCCCH + H (reaction 1b) to be the dominant channel. Unfortunately the $P(E_T)$ distribution of the C_3H_2 fragments cannot distinguish these two dissociation channels, except for the small amount of C_3H_2 + H fragments (4 ± 2%) with translational energy above the maximum for HCCCH + H products; these are presumably from the c-C_3H_2 isomer. RRKM analysis predicts that 5.6% of H loss fragments are produced as the cyclic isomer. This result is consistent with the measured translational energies of the C_3H_2 fragments, where 4 ± 2% of fragments are produced within the energetic limits of reaction 1a.

The $P(E_T)$ distribution for the C_3H + H_2 channel is quite different to that for H loss, in that it peaks well away from $E_T = 0$, dropping dramatically in intensity for $E_T < 10$ kcal/mol and showing no contribution at all for $E_T < 6$ kcal/mol. Most of the intensity lies

between translational energies of 10-20 kcal/mol, with a high energy tail extending to the maximum value of E_T ($E_{T,max}$ = 26.8 kcal/mol) for linear C_3H products. This distribution is characteristic of a dissociation channel with an exit barrier. The cutoff in the $P(E_T)$ distribution at E_T < 10 kcal/mol nearly coincides with the calculated exit barrier height[25] of 10.2 kcal/mol with respect 2-propynylidene + H_2 products (reaction 2). Such a result is consistent with a late transition state where the energy gained from passing over the barrier is channeled primarily into translation of the fragments, rather than internal degrees of freedom. The calculated transition state geometry[25] for H_2 elimination shows the geometry of the C_3H moiety to be similar to that calculated for the C_3H product,[31] a result consistent with a late transition state. The dynamics of H_2 loss from propargyl appear to the analogous channels in closed-shell hydrocarbons such as allene, propyne, and butadiene, for which the $P(E_T)$ distributions also are consistent with late exit barriers.[35,38]

Our experiments show no evidence of the lower dissociation threshold of propargyl radicals measured by McCunn *et al*[20] in the 157 nm photodissociation of propargyl chloride. According to the analysis in that study, propargyl radicals left with internal energies greater than 71.5 kcal/mol spontaneously dissociated via both H and H_2 loss, a value considerably lower than the lowest calculated dissociation asymptote, 82.4 kcal/mol for reaction 1a (*c*-C_3H_2 + H).[25] As pointed out above, our $P(E_T)$ distributions for both H and H_2 loss are consistent with the calculated thermochemical values given in Section I and extend to the maximum translational energies allowed by these values. For the lower dissociation threshold of McCunn et al to be correct, the fastest C_3H_2 fragments we observe would need to have 10.9 kcal/mol of internal energy. Such a result is theoretically possible and has been seen in the 193nm photodissociation of 1,2-butadiene.[46] However, in most

other closed shell systems of similar size the translational energy distribution for H atom loss extends to the maximum allowed value.[35,38,47]

Conclusions

Propargyl radicals, produced in the 193 nm photolysis of allene molecules in a supersonic beam, were photodissociated at 248 nm. The dissociation products were characterized by photofragment translational spectroscopy. Two channels were observed: H loss and H_2 loss, through observation of the C_3H_2 and C_3H counterparts. $P(E_T)$ distributions of the photofragments indicate that following excitation to the excited electronic state, rapid internal conversion to the ground electronic state occurs whereupon the propargyl radical dissociates in a statistical process. This study is consistent with previous measurements[19] of the H atom loss channel from propargyl in which the H atom, rather than the C_3H_2 fragment, was detected, but the H_2 channel could not have been seen in the earlier work. We find the intrachannel branching ratio for H loss/H_2 loss to be 97.6/2.4 ± 1.2, a result in good agreement with previous RRKM results.

Acknowledgements

This work was supported by the Director, Office of Basic Energy Sciences, Chemical Sciences Division of the U. S. Department of Energy under contract No. DE-AC02-05CH11231.

References

[1] R. I. Kaiser, Y. T. Lee, and A. G. Suits, J. Chem. Phys. **105** (19), 8705 (1996).

[2] R. I. Kaiser and A. M. Mebel, Int. Rev. Phys. Chem. **21** (2), 307 (2002).

[3] C. A. Taatjes, S. J. Klippenstein, N. Hansen, J. A. Miller, T. A. Cool, J. Wang, M. E. Law, and P. R. Westomoreland, Phys. Chem. Chem. Phys. **7**, 806 (2005).

[4] I. Cherchneff and J. R. Barker, Astrophys. J. **394**, 703 (1992).

[5] I. Cherchneff, J. R. Barker, and A. G. G. M. Tielens, Astrophys. J. **401**, 269 (1992).

[6] C. L. Morter, S. K. Farhat, J. D. Adamson, G. P. Glass, and R. F. Curl, J. Phys. Chem. **98**, 7029 (1994).

[7] K. Tanaka, Y. Sumiyoshi, Y. Ohshima, Y. Endo, and K. Kawaguchi, J. Chem. Phys. **107** (8), 2728 (1997).

[8] K. Tanaka, T. Harada, K. Sakaguchi, K. Harada, and T. Tanaka, J. Chem. Phys. **103** (15), 6450 (1995).

[9] L. Yuan, J. DeSain, and R. F. Curl, J. Mol. Spectrosc. **187** (1), 102 (1998).

[10] D. A. Ramsay and P. Thistlethwaite, Can. J. Phys. **44** (7), 1381 (1966).

[11] A. Fahr, P. Hassanzadeh, B. Laszlo, and R. E. Huie, Chem. Phys. **215**, 59 (1997).

[12] A. Fahr and A. H. Laufer, J. Phys. Chem. A **109**, 2534 (2004).

[13] J. M. Oakes and G. B. Ellison, J. Am. Chem. Soc. **105** (10), 2969 (1983).

[14] M. S. Robinson, M. L. Polak, V. M. Bierbaum, C. H. Depuy, and W. C. Lineberger, J. Am. Chem. Soc. **117** (25), 6766 (1995).

[15] F. P. Lossing, Can. J. Chem. **50** (24), 3973 (1972).

[16] D. W. Minsek and P. Chen, J. Phys. Chem. **94** (22), 8399 (1990).

[17] T. Gilbert, R. Pfab, I. Fischer, and P. Chen, J. Chem. Phys. **112** (6), 2575 (2000).

[18] W. M. Jackson, D. S. Anex, R. E. Continetti, B. A. Balko, and Y. T. Lee, J. Chem. Phys. **95** (10), 7327 (1991).

[19] H.-J. Deyerl, I. Fischer, and P. Chen, J. Chem. Phys. **111** (8), 3441 (1999).

[20] L. R. McCunn, B. L. FitzPatrick, M. J. Krisch, L. J. Butler, L. Chi-Wei, and J. J.-M. Lin, J. Chem. Phys. **125**, 133306 (2006).

[21] H. Honjou, M. Yoshimine, and J. Pacansky, J. Phys. Chem. **91** (17), 4455 (1987).

[22] P. Botschwina, R. Oswald, J. Flugge, and M. Horn, Zeitschrift Fur Physikalische Chemie-International Journal of Research in Physical Chemistry & Chemical Physics **188**, 29 (1995).

[23] L. Vereecken, K. Pierloot, and J. Peeters, J. Chem. Phys. **108** (3), 1068 (1998).

[24] X. Krokidis, N. W. Moriarty, W. A. Lester, and M. Frenklach, Chem. Phys. Lett. **314** (5-6), 534 (1999).

[25] T. L. Nguyen, A. M. Mebel, and R. I. Kaiser, J. Phys. Chem. A **105**, 3284 (2001).

[26] T. L. Nguyen, A. M. Mebel, S. H. Lin, and R. I. Kaiser, J. Phys. Chem. A **105**, 11549 (2001).

[27] W. Eisfeld, Phys. Chem. Chem. Phys. **7**, 3924 (2005).

[28] W. Eisfeld, J. Phys. Chem. A **110**, 3903 (2006).

[29] S. A. Wheeler, K. A. Robertson, W. D. Allen, H. F. Schaefer III, Y. J. Bomble, and J. F. Stanton, J. Phys. Chem. A **111**, 3819 (2007).

[30] It should be noted that the most recent high level calculations on propargyl radical yield a heat of formation of 85.76 kcal/mol, (ref. 29) a value 0.26 kcal/mol greater

than the value suggested by Nguyen et al. However, no revised heats of formation for the propargyl fragments were given.

[31] C. Ochsenfeld, R. I. Kaiser, Y. T. Lee, A. G. Suits, and M. HeadGordon, J. Chem. Phys. **106** (10), 4141 (1997).

[32] S. M. Sheehan, B. F. Parsons, J. Zhou, E. Garand, T. A. Yen, D. T. Moore, and D. M. Neumark, J. Chem. Phys. (in press).

[33] R. H. Qadiri, E. J. Feltham, E. E. Cottrill, N. Taniguchi, and M. N. R. Ashfold, J. Chem. Phys. **116** (3), 906 (2002).

[34] R. H. Qadiri, F. E. J., N. N. Hendrik, P. Garcia, Rodrigo, and N. R. Ashfold Michael, J. Chem. Phys. **119** (24), 12842 (2003).

[35] J. C. Robinson, N. E. Sveum, S. J. Goncher, and D. M. Neumark, Mol. Phys. **103** (13), 1765 (2005).

[36] J. W. Rabalais, J. M. McDonald, V. Scherr, and S. P. McGlynn, Chem. Rev. **71** (1), 73 (1971).

[37] D. J. Krajnovich, University of California at Berkeley, 1983.

[38] J. C. Robinson, S. A. Harris, W. Sun, N. E. Sveum, and D. M. Neumark, J. Am. Chem. Soc. **124** (34), 10211 (2001).

[39] Y. T. Lee, J. D. McDonald, P. R. LeBreton, and D. R. Herschbach, Rev. Sci. Instrum. **40** (11), 1402 (1969).

[40] J. B. Anderson and F. B. Fenn, Physics of Fluids **8** (5), 780 (1965).

[41] A. Kantrowitz and J. Grey, Rev. Sci. Instrum. **22** (5), 328 (1951).

[42] F. Z. Chen, D. L. Judge, and C. Y. R. Wu, Chem. Phys. **260**, 215 (2000).

[43] S. A. Harich, Photran (2003).

[44] W. L. Fitch and A. D. Sauter, Anal. Chem. **55** (6), 832 (1983).

[45] A. M. Schmoltner, University of California at Berkeley, 1989.

[46] J. C. Robinson, W. Sun, S. A. Harris, F. Qi, and D. M. Neumark, J. Chem. Phys. **115** (18), 8359 (2001).

[47] B. A. Balko, J. Zhang, and Y. T. Lee, J. Chem. Phys. **97** (2), 935 (1992).

Figure Captions

Figure 1: Diagram of the experimental setup, showing the pulsed beam valve, the photolysis laser at 193 nm for generating radicals, the mechanical chopper wheel, the dissociation laser at 248 nm, and the rotatable mass spectrometer for product detection.

Figure 2: Velocity distribution of propargyl radicals measured by integration of photodissociation signal over a range of different laser delays. Points indicate the measured results, while the grey line shows the least squares fit of the data using Eq. 3.

Figure 3: Representative TOF spectra of m/e = 38 ($C_3H_2^+$) fragments taken at Θ_{lab} = 7.5°, 10°, and 15°. No signal was observed for larger angles. Open circles represent the data, while the solid grey line shows the simulation based on the $P(E_T)$ distribution shown in Fig. 7a.

Figure 4: Representative TOF spectra of m/e = 37 (C_3H^+) and m/e = 36 (C_3^+) fragments taken at Θ_{lab} = 10.0°, 12.5°, and 20°. Open circles represent the data, while the grey and

dashed lines show simulated TOF spectra from the $P(E_T)$ distribution in Fig. 7a and Fig. 8, respectively. The solid black solid line shows the summed simulations, where necessary.

Figure 5: Newton diagram showing the maximum center-of-mass velocities of propargyl photodissociation products. The vector represents the lab frame velocity of propargyl radicals, and for this diagram, was set to 1535 m/s. The black circle represents c-C_3H_2 + H fragments (reaction 1a), the grey circle represents HCCCH + H fragments (reaction 1b), and the dashed circle represents HCCC + H_2 fragments (reaction 2). The maximum laboratory scattering angles for various products from propargyl radicals with a lab frame velocity of 1535 m/s are shown.

Figure 6: Representative TOF spectra of m/e = 38 (C_3D^+) taken at Θ_{lab} = 10.0°, 12.5°, and 17.5° taken during the photodissociation of C_3D_3. Contributions are marked similarly as in Fig. 4.

Figure 7: (a) $P(E_T)$ distribution for propargyl dissociation at 248 nm, including error bars, of C_3H_2 fragments used to simulate the solid grey contribution to TOF data in Figs. 3,4 and 6. The top axis shows the corresponding intenal energy of C_3H_2 fragment. The arrow at E_T = 29.7 kcal/mol shows the maximum translational energy possible for H loss products. The arrow at E_T = 15.2 kcal/mol shows where the HCCCH + H dissociation limit becomes energetically feasible. (b) Same plot for H fragment distribution determined by Deyerl *et al* for dissociation at 242 nm given for comparison between the two experiments.

Figure 8: $P(E_T)$ distribution for H_2 loss used to simulate the dashed line contribution to the TOF data in Figs. 4 and 6, including error bars. The top horizontal axis indicates the corresponding internal energy (E_{int}) of the fragments for each given translational energy. The arrow at E_T = 26.8 kcal/mol represents the maximum translational energy possible for this channel assuming production of linear C_3H.

Figure 1:

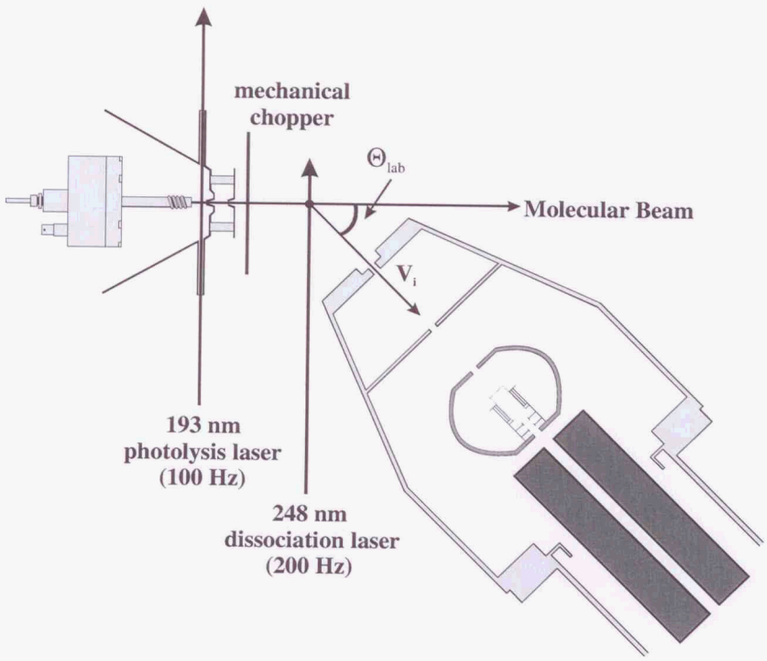

Figure 2:

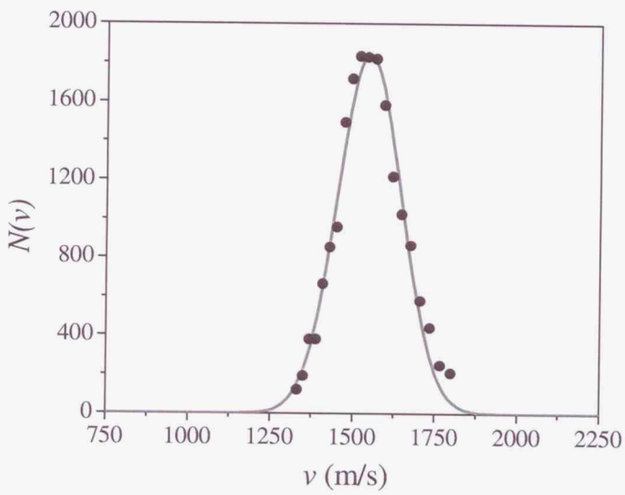

Figure 3:

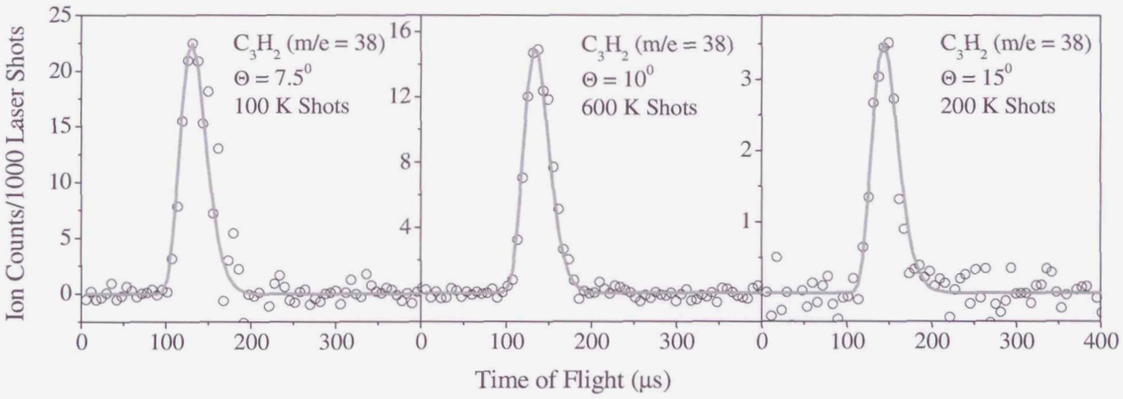

Figure 4:

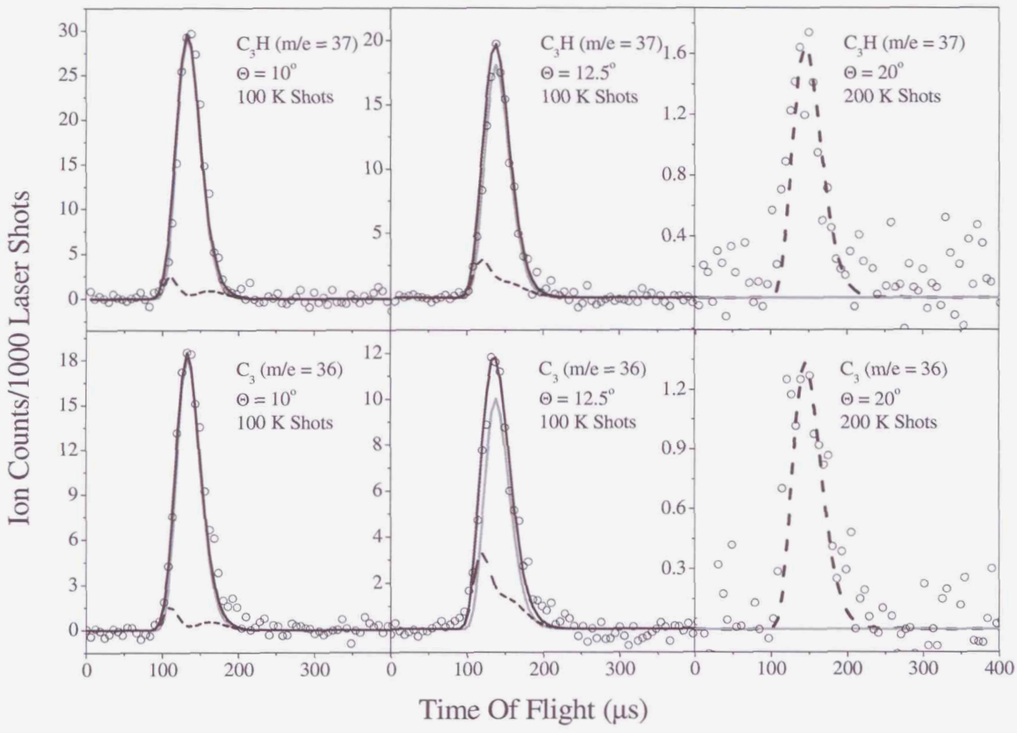

Figure 5:

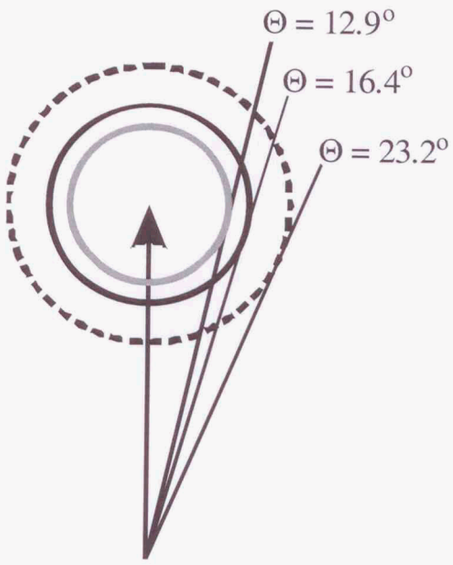

Figure 6:

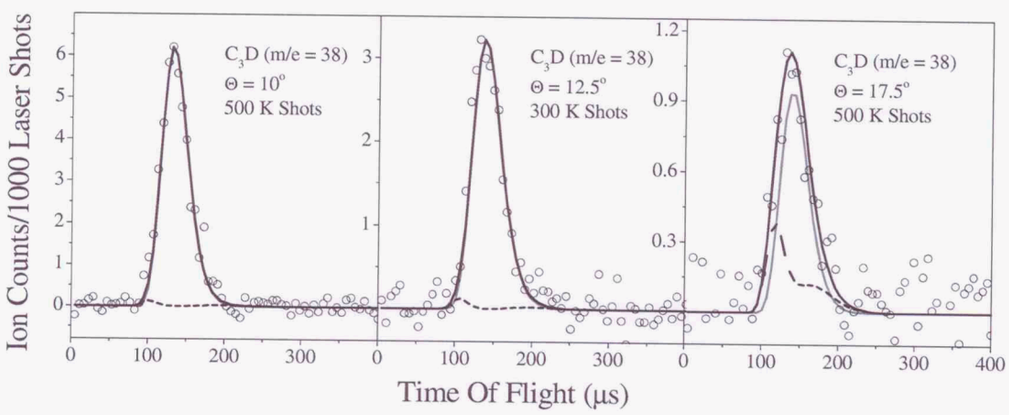

Figure 7:

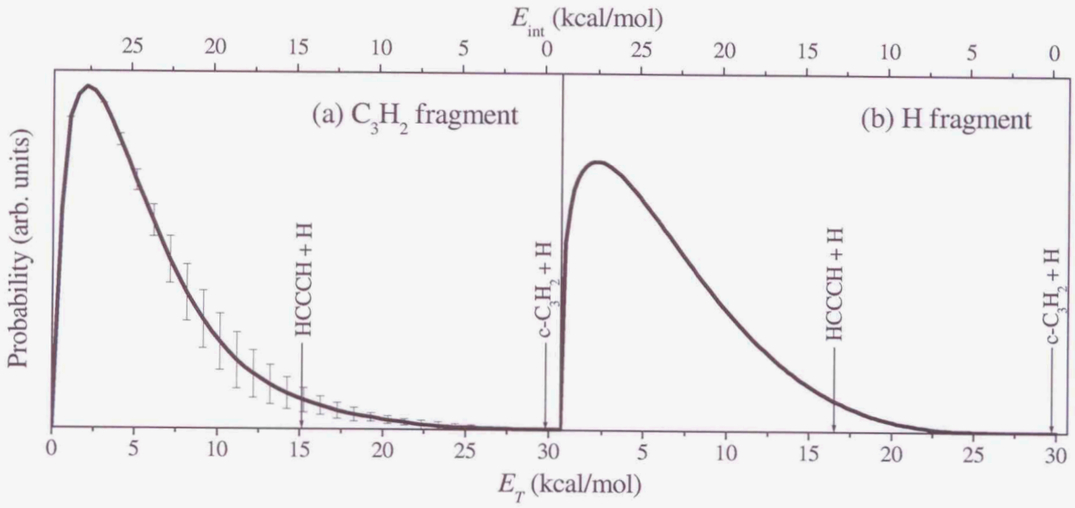
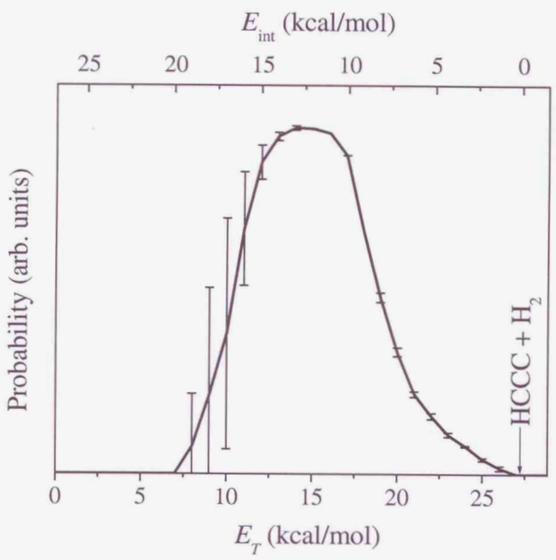
Figure 8: